Earth and Planetary Science Letters 495 (2018) 174–184

Contents lists available at ScienceDirect

Earth and Planetary Science Letters

www.elsevier.com/locate/epsl

Did climate changes trigger the Late Devonian Kellwasser Crisis? Evidence from a high-resolution conodont $\delta^{18}O_{PO_4}$ record from South China

Cheng Huang [a,c], Michael M. Joachimski [b], Yiming Gong [c,*]

[a] State Key Laboratory of Oil and Gas Reservoir Geology and Exploitation, Key Laboratory of Carbonate Reservoir of CNPC, Southwest Petroleum University, Chengdu 610500, China
[b] GeoZentrum Nordbayern, Universität Erlangen-Nürnberg, Schlossgarten 5, 91054 Erlangen, Germany
[c] State Key Laboratory of Biogeology and Environmental Geology, School of Earth Sciences, China University of Geosciences, Wuhan 430074, China

ARTICLE INFO

Article history:
Received 24 May 2017
Received in revised form 26 April 2018
Accepted 8 May 2018
Available online 25 May 2018
Editor: H. Stoll

Keywords:
Devonian
oxygen isotope
conodont
palaeotemperature
South China

ABSTRACT

The impact of climate change on biodiversity has been the focus of studies on the Phanerozoic biotic crises. However, it is still controversial whether climate change has caused the Frasnian–Famennian (F–F) biotic crisis since there is no unequivocal view on the global climate change during this critical period. In order to reconstruct palaeotemperatures during the F–F transition in South China (eastern Palaeotethys), a high-resolution oxygen isotope ($\delta^{18}O_{PO_4}$) record was obtained based on 104 measurements of conodont apatite from the Yangdi section. The oxygen isotope record based on mono-generic samples reveals an increase in $\delta^{18}O_{PO_4}$ by 0.7‰ in the Lower Kellwasser horizon (LKH) and 1.4‰ in the Upper Kellwasser horizon (UKH), translating into low-latitude surface water cooling of ~3 °C and ~6 °C, respectively. These two $\delta^{18}O_{PO_4}$ shifts agree well with the time-equivalent $\delta^{18}O_{PO_4}$ records from the western Palaeotethys, suggesting that two climate cooling pulses in conjunction with the deposition of the Kellwasser horizons are a global signal during the F–F transition. The positive shift of $\delta^{18}O_{PO_4}$ coincides with positive excursion in carbon isotope of carbonates ($\delta^{13}C_{carb}$) in the UKH, indicating that enhanced burial of organic carbon resulted in a drop in atmospheric pCO_2 and thus global climate cooling. Cooling started immediately before the Upper Kellwasser biotic crisis, with the lowest temperature documented at the top of the UKH. Climate cooling during the deposition of the LKH is observed in conjunction with the sharp decline in metazoan reefs. The coincidence of cooling and the Kellwasser biotic crisis suggests that global cooling played a major role in the collapse of ecosystems.

1. Introduction

The Late Devonian Frasnian–Famennian (F–F) biotic crisis, which is also known as the Kellwasser Crisis, represents one of the "Big Five" Phanerozoic biodiversity crises (McGhee, 1996; Stigall, 2012). This crisis severely affected the tropical marine ecosystems, especially shallow-water faunas and metazoan reefs (McGhee, 1996; Ma et al., 2016). Various mechanisms including extraterrestrial impact, oceanic anoxia, eustatic sea-level changes, oceanic eutrophication, hydrothermal activity, as well as climate changes have been proposed as potential causes (e.g. Johnson et al., 1985; Joachimski and Buggisch, 1993, 2002; Gong et al., 2002; Sandberg et al., 2002; Chen et al., 2005). Although there is no general agreement on the ultimate cause of the crisis, an increasing number of observations suggest that the F–F faunal crisis was a prolonged, multi-causal event caused by Earth-bound mechanisms (McGhee, 1996; Stigall, 2012; Ma et al., 2016). Recently, an increasing number of studies suggested that climate changes played an overarching role in major bio-events during the Phanerozoic (Finnegan et al., 2011; Trotter et al., 2015). This viewpoint has been proposed as well for the Kellwasser event based on the temporal coincidence between biodiversity fluctuation and climate change (Streel et al., 2000; Joachimski and Buggisch, 2002). However, there is no unequivocal view on the climate change during this critical period with warming (Retallack et al., 2009) and cooling (Streel et al., 2000; Joachimski and Buggisch, 2002; Balter et al., 2008) being suggested.

Oxygen isotope ratios of biogenic apatite ($\delta^{18}O_{PO_4}$) are considered as a robust palaeothermometer with only minor concerns about a diagenetic alteration and have been used to infer

* Corresponding author.
E-mail address: ymgong@cug.edu.cn (Y.M. Gong).

https://doi.org/10.1016/j.epsl.2018.05.016
0012-821X/

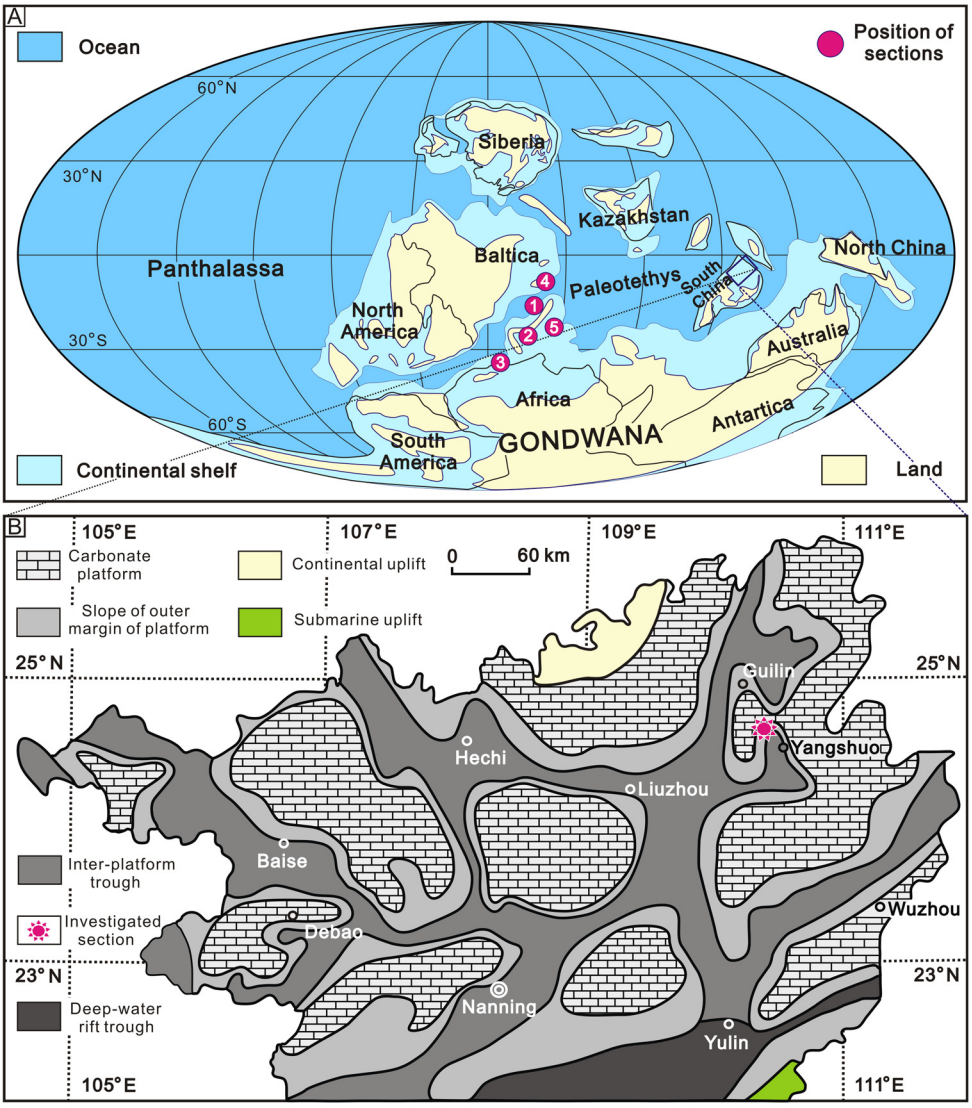

Fig. 1. (A) Late Devonian palaeogeography (modified after Joachimski et al., 2009) showing location of sections studied for $\delta^{18}O_{PO_4}$ of conodonts; 1—Vogelsberg Quarry and Behringhäuser Tunnel (Germany; Joachimski and Buggisch, 2002); 2—Coumiac and La Serre (France; Balter et al., 2008); 3—M'rirt (Morocco; Houedec et al., 2013); 4—Kowala (Poland; Joachimski et al., 2009); 5—Wolayer See (Austria; Joachimski et al., 2009). (B) Palaeogeography of Guangxi Province (South China) during the Late Devonian and location of the studied Yangdi section (modified after Xu et al., 2008). (For interpretation of the colors in the figure(s), the reader is referred to the web version of this article.)

the Devonian palaeotemperatures (Joachimski and Buggisch, 2002; Balter et al., 2008; Joachimski et al., 2009). The F–F palaeotemperature record, witnessed two short-term cooling pulses in conjunction with the deposition of the Kellwasser horizons at the western margin of the Palaeotethys, i.e., central Europe and Morocco (Joachimski and Buggisch, 2002; Balter et al., 2008; Houedec et al., 2013) (Fig. 1A). However, these records derive from relatively condensed sections and potentially cannot capture the full variance in palaeotemperature. Conversely, the F–F sections in South China, which during the Late Devonian were located at the eastern margin of the Palaeotethys, preserved relatively thick sedimentary records with abundant conodonts (Huang and Gong, 2016), adequate for constructing high-resolution palaeotemperature curves for this critical time interval. On the other hand, according to lithological and mineralogical indicators that have climatic implications, central Europe and Morocco were assigned to the arid and warm temperate palaeoclimatic zone, respectively, while South China was assigned to the tropical zone (Boucot et al., 2013, p. 73, Map 9). It is uncertain whether this difference will be documented in the corresponding palaeotemperature records.

Although palaeotemperature studies using oxygen isotopic composition of calcitic brachiopod shells have been reported from South China (Van Geldern et al., 2006), the data are too sparse to reconstruct full and detailed palaeotemperature changes during the F–F transition. Most importantly, biogenic calcite is more prone to post-depositional alteration in comparison to biogenic apatite (Joachimski et al., 2009). Accordingly, to date no detailed record for palaeotemperature changes across the F–F transition is available for South China. In order to reconstruct high-resolution palaeotemperature history during the F–F transition and to evaluate its influence on the Late Devonian ecosystems, we analyzed $\delta^{18}O_{PO_4}$ of conodonts apatite from the Yangdi section (Guangxi, South China) and compared the reconstructed temperature evolution with time-equivalent fluctuations in marine biodiversity.

2. Geological setting

The Yangdi section (24°58.2′N, 110°22.8′E) is exposed in a road cut ~35 km southeast of Guilin city, Guangxi province, South China (Fig. 1B). During the Late Devonian, the area represented a

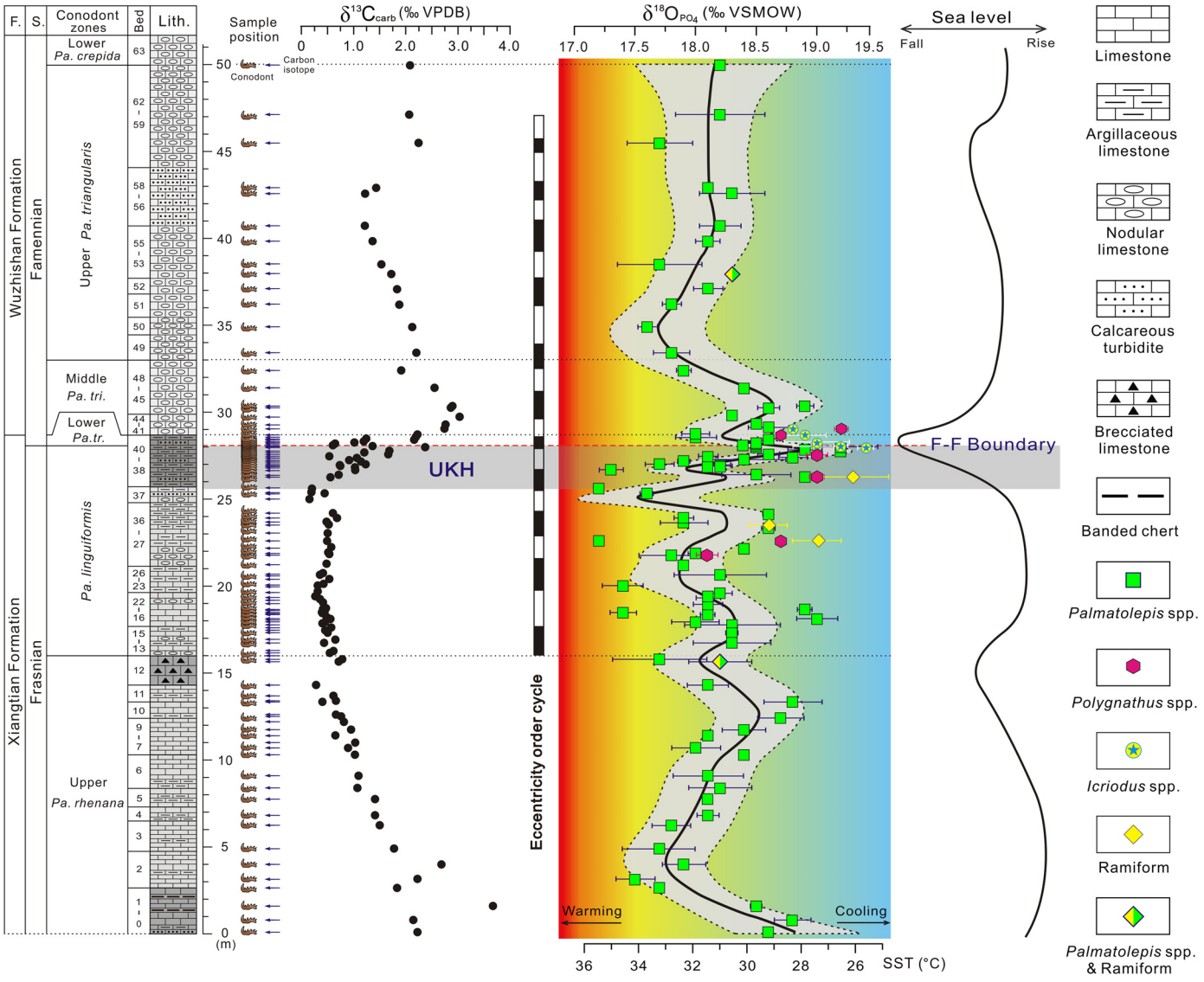

Fig. 2. Variations of $\delta^{18}O_{PO_4}$, $\delta^{13}C_{carb}$ and sea level across the F–F transition in the Yangdi section, Guangxi, South China. The $\delta^{18}O_{PO_4}$ trend was calculated by Locfit regression (solid line) with 95% confidence interval (light gray band). Horizontal bars give analytical reproducibility (1σ) for $\delta^{18}O_{PO_4}$. Vertical bars of eccentricity-forcing cycles (~100 kyr in duration) are from Chen et al. (2005). Sea-level changes modified from Ma et al. (2016). Sea surface water temperatures were calculated using the equation of Lécuyer et al. (2013), assuming a $\delta^{18}O$ value for the Late Devonian seawater of −1‰ VSMOW. F.—Formation; S.—Stage; Lith.—Lithology; *Pa.*—*Palmatolepis*; *tr.*—*triangularis*; VSMOW—Vienna standard mean ocean water; VPDB—Vienna Peedee belemnite; SST—sea surface water temperature; UKH—Upper Kellwasser horizon; LKH—Lower Kellwasser horizon.

transitional zone from a carbonate platform to an inter-platform trough in the eastern equatorial Palaeotethys (Huang and Gong, 2016). The epicontinental sea of the South China plate opened to the west into the Palaeotethys, suggesting that the studied location represented an open-marine setting.

The studied F–F succession in the Yangdi section is represented by the Xiangtian Formation and the lower part of the Wuzhishan Formation (Fig. 2). The Xiangtian Formation (late Frasnian) consists of gray thin- to thick-bedded micritic and marly limestones intercalated with calciturbidites and brecciated limestones, which may represent a slope depositional setting. The Wuzhishan Formation (Famennian) is composed of light gray thick-bedded nodular limestones. High-resolution conodont biostratigraphy of the Yangdi section was established by Huang and Gong (2016). The Upper Kellwasser horizon (UKH) has been identified in the uppermost part of the Xiangtian Formation based on a pelagic fauna turnover (e.g. elimination of the Frasnian palmatolepid and ancyrodellid conodonts, and dramatic reduction of ostracods and tentaculites), a significant positive carbon isotope excursion, as well as conodont biofacies change (Huang and Gong, 2016). However, the Lower Kellwasser horizon (LKH) in this section has not been well constrained yet since there is no deposition of dark gray bituminous limestones and black shales in the Upper *Palmatolepis rhenana* Zone.

According to cyclostratigraphy, the cyclothems (bundle, bundleset, and superbundleset) with stable hierarchical structures, ratio relationships and arrangement order were controlled by Milankovitch cyclic forcing (Gong et al., 2001). Hierarchically organized bundles, bundlesets, and superbundlesets correspond to obliquity, eccentricity, and long eccentricity cycles, respectively (Gong et al., 2001). Accordingly, the time resolution in stratigraphical sequences during the F–F transition can at least approach the order of 100 kyr since the periodicity of eccentricity (~100,000 years) remained relatively steady through geological time (Gong et al., 2001; Chen et al., 2005). Based on high-resolution conodont biostratigraphy (Huang and Gong, 2016) and cyclostratigraphy (Gong et al., 2001), the time span of the *Pa. linguiformis* Zone, Lower *Pa. triangularis* Zone, Middle *Pa. triangu-*

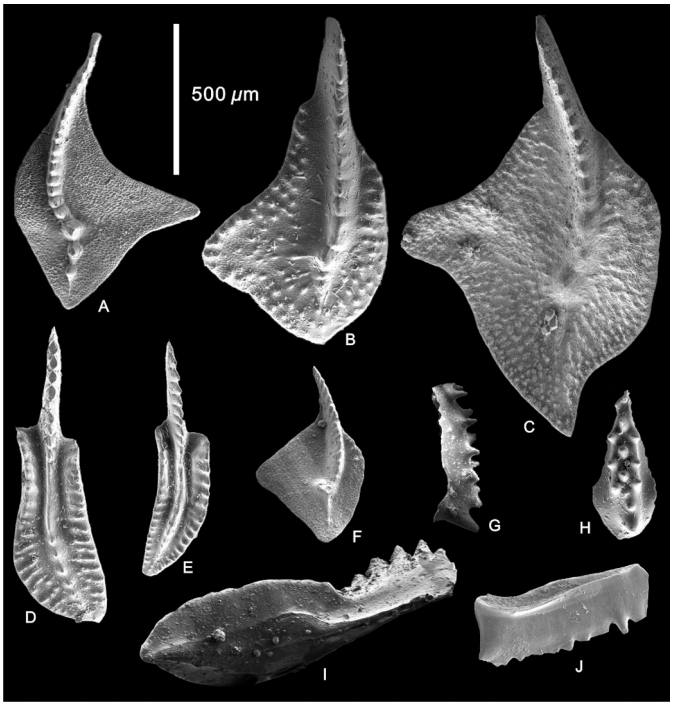

Fig. 3. Scanning electron microscope images of conodonts from the Yangdi section showing no identifiable sign of recrystallisation and basal cavity fillings. (A) *Palmatolepis hassi* Müller and Müller, from sample FA-3_002. (B) *Palmatolepis subrecta* Miller and Youngquist, FA-40D_014. (C) *Palmatolepis triangularis* Sannemann, FA-41_002. (D–E) *Polygnathus webbi* Stauffer, D, FA-40D_011; E, FA-40D_037. (F) *Palmatolepis delicatula declicatula*, Branson and Mehl, FA-41_012. (G–H) *Icriodus alternatus* Branson & Mehl, G, FA-41_019; H, FA-41_020. (I) *Polygnathus* sp., FA-41_024. (J) *Pelekysgnathus planus* Sannemann, FA-58_009.

laris Zone, and UKH, were estimated to be ∼800 kyr, ∼100 kyr, ∼300 kyr, and ∼200 kyr, respectively. Knowing the thickness of sediments deposited during the *Pa. linguiformis* Zone to Middle *Pa. triangularis* Zone, the average sedimentation rate of the Yangdi section is assumed to be around 1.4 cm/kyr.

3. Materials and methods

A total of 90 conodont samples and 109 carbon isotope samples were collected from the 50 m-thick strata spanning the Xiangtian Formation and lower part of the Wuzhishan Formation (Fig. 2). According to sampling intensity, every eccentricity-forcing bundleset (∼100 kyr) in the *Pa. linguiformis* Zone, uppermost of *Pa. linguiformis* Zone−Lower *Pa. triangularis* Zone and Middle *Pa. triangularis* Zone encompasses about 5, 10, 4 conodont samples, respectively. Thus, the time resolution of samples in these intervals is ∼20 kyr, ∼10 kyr and ∼25 kyr, respectively. For conodont extraction, carbonate rock samples were crushed into small chips and dissolved in 10% acetic acid. The acid solution was exchanged every 48 h until the rocks were completely dissolved. Residuals were wet sieved, dried at 30 °C and separated by using heavy liquid separation with lithium heteropolytungstates (2.81–2.82 g/ml).

The conodont specimens were handpicked under a stereomicroscope. More than 10,000 well-preserved conodont elements (P_1) were obtained and taxonomically identified (see details in Huang and Gong, 2016). Specimens without identifiable recrystallisation or overgrowth on the conodont surfaces were used for further processing (Fig. 3). Further, only specimens without basal cavities fillings have been selected to avoid potential diagenetic artifacts from the basal fillings composed of fine-grained apatite crystals (Wenzel et al., 2000). In order to test whether different conodont taxa vary in their oxygen isotope ratios, mono-generic assemblages of *Palmatolepis*, *Polygnathus*, *Icriodus* picked from the same sample were analyzed in case of abundant faunas. Since *Palmatolepis* is most abundant in this section, this genus was preferentially used for oxygen isotope analysis. Multi-generic conodont assemblages were used for analysis in case conodont abundance was not sufficiently high to allow mono-generic analyses.

Conodont elements (0.5–1.0 mg) were dissolved in nitric acid and the apatite phosphate group was re-precipitated as trisilverphosphate (Ag_3PO_4) following the method described in Joachimski et al. (2009). The obtained Ag_3PO_4 crystals were thoroughly rinsed with deionized water, dried at 60 °C and ground to fine powder using a small agate mortar. 0.2–0.3 mg Ag_3PO_4 powder was weighed into silver foil and transferred into the sample carousel of TC-EA (Temperature Conversion-Elemental Analyzer) coupled online to a ThermoFinnigan Delta V Plus mass spectrometer. A laboratory standard, as well as NBS 120c were used as control standards and processed together with samples. Samples and standards were generally analyzed in triplicate (Helium flow rate was 80 ml/s, reactor temperature was set to 1450 °C, column temperature was 90 °C). The $\delta^{18}O_{PO_4}$ values are reported in per mil deviation relative to VSMOW (Vienna Standard Mean Ocean Water). The analyses were calibrated by performing a two-point calibration (Paul et al., 2007) using NBS 120c (21.7‰) and a commercial Ag_3PO_4 (9.9‰). All standards were calibrated to TU1 (21.11‰) and TU2 (5.45‰; Vennemann et al., 2002). Reproducibility of replicate internal laboratory standard analyses was ±0.30‰ (1σ; $n = 17$). NBS 120c used as external standard was measured as 21.7 ± 0.26‰ (1σ, $n = 16$) (Lécuyer et al., 1993). Replicate analyses of the internal laboratory standards and NBS 120c were performed between every four samples, as well as at the start and end of each measuring day to monitor accuracy and reproducibility. All the measurements were performed in the Stable Isotope Laboratory of the GeoZentrum Nordbayern, University of Erlangen–Nuremberg, Germany.

Fresh carbonate rock samples were cut into rock slabs using a diamond blade saw. The rock slabs were polished and cleaned in ultrasonic bath to remove the surface contaminants. Powders were drilled from the cleaned rock slabs using a stainless-steel dental drill. Carbon isotope analyses of powdered whole rock carbonates ($\delta^{13}C_{carb}$) were performed using a KIEL IV device connected to a ThermoFinnigan MAT 253 mass spectrometer at the State Key Laboratory of Geological Processes and Mineral Resources, China University of Geosciences, Wuhan. All carbon isotope values are reported in per mil deviation relative to VPDB (Vienna Peedee belemnite). Accuracy of carbon isotope measurements was monitored by replicate analyses of laboratory standards and was ±0.05‰ (1σ).

Isotope trend lines (based on *Palmatolepis* spp.) were calculated using nonparametric locally weighted regression method “Locfit” (Loader, 1999), which produces a smoothed curve retaining local minima and maxima, as well as yields good results even with unevenly spaced data points. Considering the scatter in the data and the results of cross validation for different smoothing parameters (α), the fitted $\delta^{18}O_{PO_4}$ curve with $\alpha = 0.15$ is considered to represent the main trend of $\delta^{18}O_{PO_4}$ records (details in the Supplementary material). All calculations were performed with the open source statistic software ‘R’ (version 3.3.1; Ihaka and Gentleman, 1996).

4. Results

The $\delta^{18}O_{PO_4}$ values based on 104 measurements of conodonts fluctuate between 17.2 and 19.2‰ from the Upper *Pa. rhenana* to Lower *Pa. crepida* Zone (Fig. 2, detailed data are given in Supplementary material). The oxygen isotope records measured on mono-generic conodont assemblages from the same rock sample exhibit identifiable differences in average values in the Lower to Middle

Table 1
Oxygen isotope value for individual conodont genera or multi-generic assemblages. *Pa.*—*Palmatolepis*; *L.*—*Ligonodina* spp.; *N.*—*Neoprioniodus* spp.; *S.*—*Synprioniodina* spp.; *O.*—*Ozarkodina* spp. L.—Lower; M.—Middle; σ—standard deviation.

Sample	Conodont taxa	$\delta^{18}O_{PO_4}$ (‰ VSMOW)	1σ	Conodont zones
FA-42	*Palmatolepis* spp.	18.6	0.17	M. *Pa. triangularis*
FA-42	*Polygnathus* spp.	19.2	0.06	M. *Pa. triangularis*
FA-42	*Icriodus* spp.	18.8	0.04	M. *Pa. triangularis*
FA-41	*Palmatolepis* spp.	18	0.12	M. *Pa. triangularis*
FA-41	*Polygnathus* spp.	18.7	0.01	M. *Pa. triangularis*
FA-41	*Icriodus* spp.	18.9	0.18	M. *Pa. triangularis*
FA-40P	*Palmatolepis* spp.	18.5	0.12	M. *Pa. triangularis*
FA-40P	*Icriodus* spp.	19	0.27	M. *Pa. triangularis*
FA-40O	*Palmatolepis* spp.	18.4	0.02	M. *Pa. triangularis*
FA-40O	*Icriodus* spp.	19.2	0.06	L. *Pa. triangularis*
FA-40N	*Palmatolepis* spp.	18.5	0.08	L. *Pa. triangularis*
FA-40N	*Icriodus* spp.	19	0.2	L. *Pa. triangularis*
FA-40M	*Palmatolepis* spp.	19.2	0.3	L. *Pa. triangularis*
FA-40M	*Icriodus* spp.	19.4	0.07	L. *Pa. triangularis*
FA-40I	*Palmatolepis* spp.	18.6	0.09	*Pa. linguiformis*
FA-40I	*Polygnathus* spp.	19	0.07	*Pa. linguiformis*
Y38F	*Palmatolepis* spp.	18.9	0.04	*Pa. linguiformis*
Y38F	*Polygnathus* spp.	19	0.06	*Pa. linguiformis*
Y38F	Ramiform ($L.+N.+S.$)	19.3	0.29	*Pa. linguiformis*
FA-30	*Polygnathus* spp.	18.7	0.04	*Pa. linguiformis*
FA-30	Ramiform ($L.+O.+S.$)	19	0.2	*Pa. linguiformis*
FA-27B	*Palmatolepis* spp.	17.8	0.27	*Pa. linguiformis*
FA-27B	*Polygnathus* spp.	18.1	0.09	*Pa. linguiformis*

Pa. triangularis Zone. The $\delta^{18}O_{PO_4}$ values of *Palmatolepis* spp. show 0.6–0.7‰ and 0.5–0.9‰ lower than those of *Polygnathus* spp. and *Icriodus* spp., respectively (Table 1). However, platform elements (*Polygnathus* spp. and *Palmatolepis* spp.) display no identifiable difference in $\delta^{18}O_{PO_4}$ values than ramiform elements (multi-generic assemblages) taking into account an analytical precision of ±0.3‰ (1σ).

The $\delta^{18}O_{PO_4}$ values based on mono-generic samples (*Palmatolepis* spp.) show a rapid decrease in the lower part of the Upper *Pa. rhenana* Zone followed by a minor increase (~0.7‰) culminating at the top of this zone. From the topmost Upper *Pa. rhenana* Zone to the base of the UKH, average $\delta^{18}O_{PO_4}$ values are relatively homogeneous except some scattered values. A significant positive shift in $\delta^{18}O_{PO_4}$ (+1.4‰) starts slightly below the UKH with the highest value (19.2‰) encountered at the F–F boundary. During the early Famennian, two discrete decreases in $\delta^{18}O_{PO_4}$ with amplitudes of 0.7‰ and 0.9‰ are registered in the Lower *Pa. triangularis* Zone and Middle–Upper *Pa. triangularis* Zone, respectively. Subsequently, $\delta^{18}O_{PO_4}$ gradually increases to relatively uniform values around 18.1‰ during the lower to middle part of the Upper *Pa. triangularis* Zone.

The carbon isotope values fluctuate between 0.2 and 3.0‰, with an average of 1.1‰ (Fig. 2, detailed data are given in Supplementary material). Generally, the carbon isotope record shows an ongoing decrease of ~1.8‰ from the lower part of the Upper *Pa. rhenana* Zone to the base of the *Pa. linguiformis* Zone. During the *Pa. linguiformis* Zone, $\delta^{13}C_{carb}$ record reveals a relatively homogeneous distribution of values (0.3 to 0.6‰). A significant positive carbon isotope excursion (+2.6‰) starts just below the UKH and culminates in the Middle *Pa. triangularis* Zone (3.0‰). Subsequently, carbon isotope gradually decreases to values between 1.4 and 1.8‰.

5. Discussion

5.1. Preservation of primary $\delta^{18}O_{PO_4}$ signals

Conodont apatite has a high preservation potential for the primary isotopic composition due to the dense microcrystalline structure (Trotter et al., 2007). Consequently, oxygen isotope ratios in conodont phosphate are generally assumed to be relatively resistant to diagenetic alteration (Joachimski et al., 2009; Trotter et al., 2015), although they may be modified by enzyme mediated microbiological activity (Zazzo et al., 2004) or by diagenetic fluids at high temperatures (Pucéat et al., 2004). Rare earth element (REE) and Sr patterns in biogenic apatite were interpreted to reflect partially a diagenetic signal (Thomas et al., 2007). However, neither REE and trace element patterns nor cathodoluminescence characteristics are helpful in identifying a diagenetic exchange of oxygen in the phosphate ion of biogenic apatite (Buggisch et al., 2008; Joachimski et al., 2009). Although the crystallinity of biogenic apatite was initially proposed as a tool for deciphering geochemically altered apatites (Shemesh, 1990), it was later refused as a proxy for a diagenetic alteration of conodont apatite (Pucéat et al., 2004).

The conodont color alteration index (CAI) is considered as a proxy for the maximum thermal overprint (Rejebian et al., 1987), with a high thermal overprint potentially resulting in recrystallisation (aggrading neomorphism) of conodont apatite (Nöth, 1998). Although the CAI values for most conodont samples in the Yangdi section are up to 4.5 (Fig. 4), corresponding to 200 to 300 °C thermal overprint, there are no signs of recrystallisation on the conodont surfaces (Fig. 3). Several studies have shown that there is no major difference in $\delta^{18}O_{PO_4}$ values from time-equivalent conodont samples having CAI of 1 to 5 (Joachimski et al., 2009; Trotter et al., 2015) or even to 7 (Buggisch et al., 2008). The conodont $\delta^{18}O_{PO_4}$ values measured in the Yangdi section (17.2–19.2‰) are comparable to published results from sections in Germany (Behringhäuser Tunnel: 17.0–19.0‰, Vogelsberg Quarry: 17.4–19.0‰) (Joachimski and Buggisch, 2002) and France (Coumiac: 17.4–19.0‰, La Serre: 16.9–18.6‰) (Balter et al., 2008). However, these data are on average 1.3‰ higher than the records from Morocco sections (M'rirt: 15.9–17.8‰) (Houedec et al., 2013).

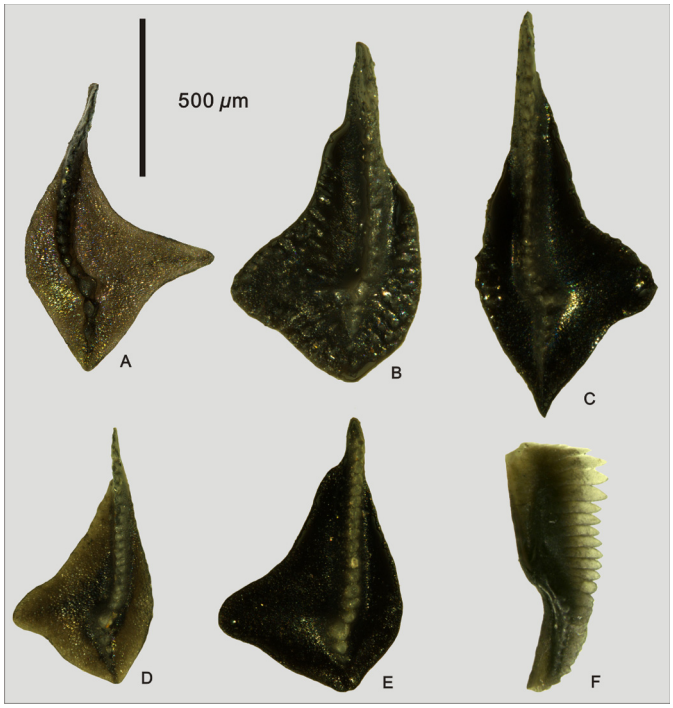

Fig. 4. Optical microscope images of conodonts from the Yangdi section showing the conodont color alteration index (CAI). (A) *Palmatolepis hassi* Müller and Müller, from sample FA-3_002, CAI = 3.5. (B) *Palmatolepis subrecta* Miller & Youngquist, FA-40D_014, CAI = 4.5. (C) *Palmatolepis gigas extensa* Ziegler and Sandberg, FA-40E_030, CAI = 4.5. (D) *Palmatolepis subrecta*, Miller and Youngquist, FA-0_015, CAI = 3.5. (E) *Palmatolepis juntianensis*, Han, FA-6_015, CAI = 4.5. (F) *Polygnathus decorosus* Stauffer, FA-40C_011, CAI = 3.5.

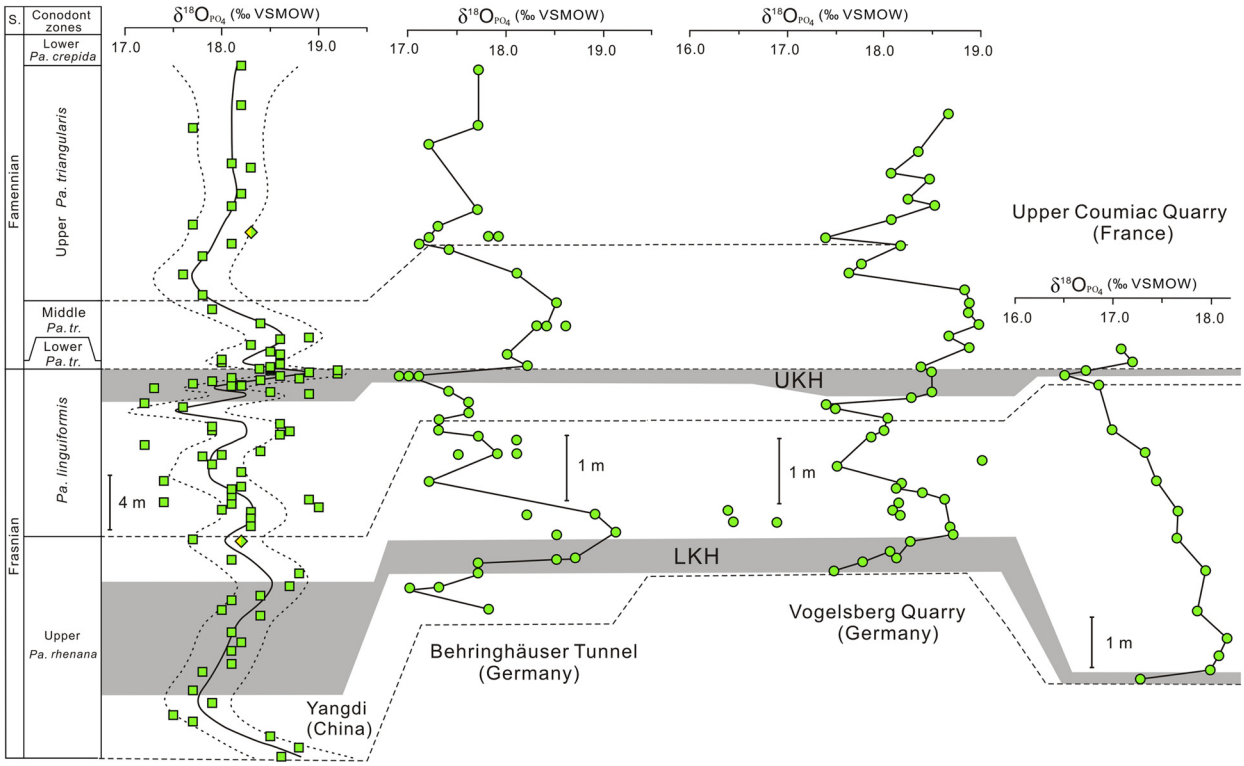

Fig. 5. Comparison of the conodont $\delta^{18}O_{PO_4}$ record from Yangdi (this study) with published $\delta^{18}O_{PO_4}$ records from Germany (Joachimski and Buggisch, 2002) and France (Balter et al., 2008). The data from France have been corrected by −0.9‰ (see text for explanation). The trend lines of $\delta^{18}O_{PO_4}$ records from European sections are drawn according to the original trend lines given in the published figures (Joachimski and Buggisch, 2002; Balter et al., 2008). Lower Kellwasser (LKH) and Upper Kellwasser horizons (UKH) are indicated by the shaded areas. S.—Stage; *Pa.*—*Palmatolepis*; *tr.*—*triangularis*.

Since the $\delta^{18}O_{PO_4}$ analyses of Balter et al. (2008) and Houedec et al. (2013) were calibrated by assigning a value of 22.4 and 22.6‰ VSMOW to standard NBS 120c, a correction of −0.7 to −0.9‰ is required in order to compare these values with the analyses performed on samples from Germany and South China (calibrated to NBS 120c = 21.7‰ VSMOW). With this correction, the $\delta^{18}O_{PO_4}$ values from France and Morocco become lower in comparison to the values measured on conodonts from South China and Germany. This discrepancy in absolute $\delta^{18}O_{PO_4}$ values probably reflects differences in local conditions (e.g. precipitation/evaporation ratio). Higher $\delta^{18}O_{PO_4}$ values are measured in lower palaeolatitudes (e.g. South China) (Fig. 1A) and are probably related to relative higher evaporation, while lower $\delta^{18}O_{PO_4}$ values are measured on conodonts from higher palaeolatitudes (e.g. La Serre and Morocco) with a higher precipitation/evaporation ratio.

The main trend in $\delta^{18}O_{PO_4}$ calculated by the Locfit regression method is comparable to published results (Joachimski and Buggisch, 2002; Balter et al., 2008; Joachimski et al., 2009; Houedec et al., 2013), especially the positive excursion in $\delta^{18}O_{PO_4}$ (~1.4‰) in the UKH can be well correlated with time-equivalent oxygen isotope records from Germany (~1.5‰) (Joachimski and Buggisch, 2002), Poland (~1.5‰), Austria (~1.5‰) (Joachimski et al., 2009), France (~1.0‰) (Balter et al., 2008) and Morocco (~1.1‰) (Houedec et al., 2013) (Fig. 5). Moreover, the $\delta^{18}O_{PO_4}$ increase (~0.7‰) in the Upper *Pa. rhenana* Zone also can be correlated with the oxygen isotope records in the LKH from German (~1.5‰), French (1.1–1.5‰) and Moroccan (~1.9‰) sections. In summary, the $\delta^{18}O_{PO_4}$ record from the Yangdi section agrees well with published results in respect to the overall trend, suggesting the primary oxygen isotope signals in most samples were preserved.

5.2. Palaeoecology of Late Devonian conodonts

Conodont animals are generally interpreted as nektonic organisms based on the preservation of tissues (e.g. body muscles, fins, notochord, and eyes) in the soft body fossils (Donoghue et al., 2000). The $\delta^{18}O_{PO_4}$ values of conodont taxa thriving in surface waters will record surface water temperatures and accordingly be helpful in deciphering climatic changes, whereas $\delta^{18}O_{PO_4}$ values of taxa dwelling deeper in the water column would record cooler temperatures. Therefore, the knowledge concerning the life style of conodonts is crucial for reconstruction of palaeotemperature using $\delta^{18}O_{PO_4}$ values of conodont apatite. Since the palaeoecology of conodont taxa is generally inferred from the sedimentological setting, the inhabited water depth of specific conodont taxa is still ambiguous, especially for pelagic taxa.

Comparable $\delta^{18}O_{PO_4}$ values were observed for the Late Devonian mono-generic samples of *Palmatolepis*, *Polygnathus*, and *Icriodus* from European sections, suggesting that all three taxa were thriving in waters with comparable water temperatures and thus at comparable water depths, i.e., upper part of water column (Joachimski and Buggisch, 2002; Joachimski et al., 2009). Similarly, taking into account an analytical reproducibility of ±0.3‰ (1σ), $\delta^{18}O_{PO_4}$ values of mono-generic elements measured in this study (i.e. *Palmatolepis* spp., and *Polygnathus* spp.) are indistinguishable in samples from the *Pa. linguiformis* Zone to the base of the Lower *Pa. triangularis* Zone at the Yangdi section (Table 1), suggesting a comparable habitat. However, in the Lower to Middle *Pa. triangularis* Zone, *Palmatolepis* spp. display 0.6–0.7‰ and 0.5–0.9‰ lower $\delta^{18}O_{PO_4}$ values than *Polygnathus* spp. and *Icriodus* spp., respectively. If only explained by temperature, these differences in $\delta^{18}O_{PO_4}$ translate into 2.3 to 4.1 °C warmer temperatures recorded by *Palmatolepis* spp. (using the equation of Lécuyer et al., 2013).

Since temperature will decrease with increasing water depth, higher $\delta^{18}O_{PO_4}$ values argue for a deeper water habitat (cooler temperatures) and vice versa. The lower $\delta^{18}O_{PO_4}$ values of *Palmatolepis* spp. suggest that *Palmatolepis* lived in shallower (warmer) waters compared to *Polygnathus* and *Icriodus*. However, as indicated by conodont biofacies, species of *Palmatolepis* are generally associated with open-marine pelagic (offshore) sediments, while *Polygnathus* and *Icriodus* preferentially occur in shallow water (or near shore) deposits (Sandberg et al., 1989). The water-depths inferred from $\delta^{18}O_{PO_4}$ records are in conflict with traditional conodont biofacies models (e.g. Sandberg et al., 1989). This is because the recorded differences in $\delta^{18}O_{PO_4}$ of mono-generic samples are observed in an unusual palmatolepid–icriodid mixed biofacies (see conodont biofacies in Huang and Gong, 2016), which implies that the inhabited water depth of conodonts (i.e. *Icriodus* spp.) is distinct from the traditional ecological models inferred from the sedimentological setting.

Most Frasnian pelagic conodont taxa were decimated by the F–F biotic crisis and left vacant ecospace, whereas all icriodids and a few polygnathids taxa survived the crisis (Sandberg et al., 1989) and may have expanded into a range of environments normally not occupied by them. This ecological expansion could have resulted in the special palmatolepid–icriodid mixed biofacies, which is not represented in traditional biofacies models (e.g. Sandberg et al., 1989). It has been observed that the rapid evolutionary changes in conodont fauna affected conodont biofacies distributions during the F–F biotic crisis in eastern Anti-Atlas, Morocco (Belka and Wendt, 1992). The world-wide distribution of palmatolepid–icriodid mixed biofacies (e.g. Sandberg et al., 1989; Belka and Wendt, 1992; Huang and Gong, 2016) makes it difficult to explain this mixed biofacies as a result of reworking. We argue that the $\delta^{18}O_{PO_4}$ data support the interpretation that palmatolepid–icriodid mixed biofacies developed by telescoping of the niches of palmatolepids and icriodids after elimination of niches of other taxa (Sandberg et al., 1989). In summary, we suggest that both *Polygnathus* and *Icriodus* could live at variable water-depths (shallow to deeper water), whereas *Palmatolepis* was likely to live in the upper part of water column. As a result, the $\delta^{18}O_{PO_4}$ record of *Palmatolepis* is more suitable for reconstructing sea surface water temperature (SST).

5.3. Palaeotemperature changes during the F–F transition

The oxygen isotope composition of biogenic apatite is dependent on temperature and the $\delta^{18}O$ value of seawater ($\delta^{18}O_{seawater}$) from which apatite precipitates (Kolodny et al., 1983; Pucéat et al., 2010; Lécuyer et al., 2013). The latter is a function of salinity, ice volume and is potentially influenced by secular changes in $\delta^{18}O_{seawater}$ (Veizer and Prokoph, 2015). Considering the ice-volume effect on the oxygen isotopic composition of modern sea water $\delta^{18}O$ (e.g. Savin, 1977), a $\delta^{18}O_{seawater}$ value of $-1‰$ is generally assumed for open-marine waters in an ice-free world (e.g. Devonian; Joachimski et al., 2009). However, enhanced evaporation will result in higher salinities and elevated $\delta^{18}O$ values, while elevated rainfall exceeding evaporation rate will lead to lower salinities and lower $\delta^{18}O$ values.

Some authors suggested that the oxygen isotopic composition of ocean became depleted in ^{18}O with increasing age based on the oxygen isotope records of the Phanerozoic calcitic fossils (Veizer and Prokoph, 2015). This potential secular change in $\delta^{18}O_{seawater}$ has been supported by geological modeling (Jaffrés et al., 2007). However, other authors claim that $\delta^{18}O_{seawater}$ was buffered by hydrothermal and weathering processes within a range of $0 \pm 2‰$ throughout Earth history (e.g. Muehlenbachs, 1998; Lécuyer and Allemand, 1999). Carbonate clumped isotopes revealed that the $\delta^{18}O$ value of the Phanerozoic seawater was invariant over the last ~500 million years with an average value of $-0.8‰$ VSMOW (Henkes et al., 2018). Although the calculation of absolute temperatures is hampered by the uncertainty in $\delta^{18}O_{seawater}$, relative temperature changes can be constrained from the general trends and amplitudes of changes in $\delta^{18}O_{PO_4}$. For example, a $1‰$ shift in $\delta^{18}O_{PO_4}$ corresponds to a 4.5 °C change in temperature using the palaeotemperature equation of Lécuyer et al. (2013).

A minor $\delta^{18}O_{PO_4}$ increase (~0.7‰) starting at the lower part of the Upper *Pa. rhenana* Zone in the Yangdi section can be correlated with the positive shift in $\delta^{18}O_{PO_4}$ (1.1–1.9‰) associated with the LKH in the western Palaeotethys (Joachimski and Buggisch, 2002; Balter et al., 2008; Houedec et al., 2013) (Fig. 5), suggesting that the $\delta^{18}O_{PO_4}$ increase associated with the LKH is a global signal. The minor $\delta^{18}O_{PO_4}$ increase (~0.7‰) in the Yangdi section translates into about 3 °C cooling. The onset of the climatic cooling associated with the LKH varied from the top of the Lower *Pa. rhenana* Zone (e.g. M'rirt section, Morocco; Houedec et al., 2013) to the lower part of the Upper *Pa. rhenana* Zone (e.g. Behringhäuser Tunnel section, Germany; Joachimski and Buggisch, 2002) in different areas, the timing of which can be roughly correlated with the demise of metazoan reefs (Copper, 2002). As the $\delta^{18}O_{PO_4}$ increase occurs in a succession with thickness of ~10 m, the duration of the cooling associated with the LKH was estimated to be around 700 kyr assuming the sedimentation rate of the succession in the Yangdi section is constant.

During the F–F transition, the significant $\delta^{18}O_{PO_4}$ increase of ~1.4‰ in the UKH agrees well with published $\delta^{18}O_{PO_4}$ records (1.0–1.5‰) from the western Palaeotethys (Joachimski and Buggisch, 2002; Balter et al., 2008; Joachimski et al., 2009; Houedec et al., 2013), suggesting that it represents as well a global signal. Furthermore, an increase (~1‰) in $\delta^{18}O$ measured on well-preserved brachiopod calcite was also observed in the succession across the F–F boundary from different palaeocontinents (i.e. South China, Siberia, and Northern Gondwana; Van Geldern et al., 2006). As the studied area was located in an open-marine setting far from any major continent (Fig. 1), salinity is considered not to be influenced by extreme evaporation or enhanced freshwater input. This is supported by the observation that conodonts (Huang and Gong, 2016) and brachiopods (Xu et al., 2008) occurred throughout the studied section, suggesting that a significant change in surface water salinity is implausible. Consequently, the positive shift of $\delta^{18}O_{PO_4}$ in the UKH is explained as a temperature change.

Previously, the 1.0–1.5‰ increase in $\delta^{18}O_{PO_4}$ was interpreted as climate cooling of low-latitude surface waters by 5–7 °C (Joachimski and Buggisch, 2002), thus the 1.4‰ increase measured in this study corresponds to ~6 °C cooling if explained exclusively by a change in surface water temperature. Climate cooling indicated by higher $\delta^{18}O_{PO_4}$ values during the F–F transition is also consistent with the reduced miospore diversity in continental areas (Streel et al., 2000). However, the amplitude of this cooling seems large in comparison to the assumed low-latitude cooling of 1–5 °C during the Pleistocene Last Glacial Maximum (LGM) (Schrag et al., 1996). The calculated palaeotemperature decrease would be reduced in case ice volume changes occurred and affected $\delta^{18}O$ of oceanic waters. The coincidence of cooling and a significant eustatic sea-level fall (Johnson et al., 1985; Sandberg et al., 2002) seems to imply a glacio-eustatic control on sea-level changes, although there is no report for glacial deposits of Frasnian to early Famennian age. Streel et al. (2000) argued that rapid formation and collapse of short-term glacier could have resulted in rapid sea-level changes, which might have destroyed the preservation of glacial deposits.

During the early Famennian, two discrete decreases in $\delta^{18}O_{PO_4}$ with amplitudes of 0.7‰ and 0.9‰ are recorded in the Lower *Pa. triangularis* Zone and Middle–Upper *Pa. triangularis* Zone, respectively, which translates into warming of about 3 and 4 °C. In

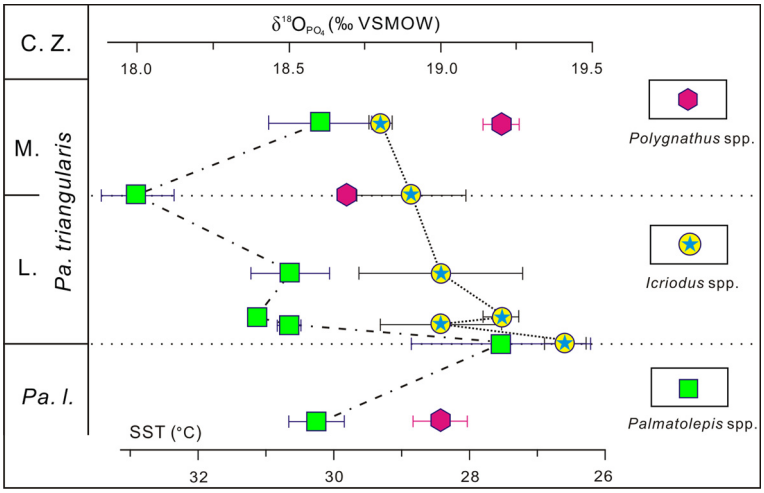

Fig. 6. Variations in $\delta^{18}O_{PO_4}$ across the F–F boundary for different conodont genera. Both *Palmatolepis* and *Icriodus* show a decreasing trend in $\delta^{18}O_{PO_4}$ during the Lower *triangularis* Zone. Horizontal bars give analytical reproducibility (1σ) for $\delta^{18}O_{PO_4}$. C. Z.—Conodont zones; L.—Lower; M.—Middle; *Pa.*—*Palmatolepis*; *l.*—*linguiformis*.

contrast to the discrete warming in South China, time-equivalent $\delta^{18}O_{PO_4}$ records from Germany (Joachimski and Buggisch, 2002) and Poland (Joachimski et al., 2009) showed that continuous cooling occupied the earliest Famennian until a successive warming started in the middle part of the Middle *Pa. triangularis* Zone. However, the minor warming during the Lower *Pa. triangularis* Zone can be observed in the time-equivalent succession in the Wolayer See (Joachimski et al., 2009) and La Serre sections (Balter et al., 2008). This warming has been documented by both *Palmatolepis* spp. and *Icriodus* spp. (Fig. 6). Although there is a difference in the two $\delta^{18}O_{PO_4}$ records from Wolayer See and La Serre presumably due to different sampling densities in the Lower *Pa. triangularis* Zone, the decrease in $\delta^{18}O_{PO_4}$ during the Middle–Upper *Pa. triangularis* Zone can be observed in different areas (Joachimski and Buggisch, 2002; Joachimski et al., 2009). This decrease in $\delta^{18}O_{PO_4}$ also agrees well with time-equivalent $\delta^{18}O$ records measured on well-preserved brachiopod calcite from South China and Siberia (Van Geldern et al., 2006), suggesting a global warming during the Middle–Upper *Pa. triangularis* Zone.

5.4. Relationship between climate changes and carbon cycle

Two positive carbon isotope ($\delta^{13}C_{carb}$) excursions of approximately +3‰ coinciding with the deposition of the Kellwasser horizons have been considered as global changes in $\delta^{13}C$ of oceanic dissolved inorganic carbon ($\delta^{13}C_{DIC}$) (Joachimski and Buggisch, 1993; Joachimski et al., 2002). The carbon isotope record of carbonates measured in the Yangdi section shows a positive shift of +2.6‰ across the F–F boundary and correlates with the UKH. This carbon isotope pattern agrees well with published results from Euramerica, Northern Gondwana (Joachimski and Buggisch, 1993; Joachimski et al., 2002), as well as other sections in South China (Chen et al., 2005). This suggests that the carbon isotope pattern across the F–F boundary at the Yangdi section has preserved global variations in $\delta^{13}C_{DIC}$.

Generally, short-term (less than ~100 kyr) changes in $\delta^{13}C_{carb}$ are related to variations in productivity whereas on a longer timescale (larger than ~100 kyr), shifts in $\delta^{13}C_{carb}$ reflect changes in burial rate of organic carbon or variation of the riverine carbon input (e.g. Joachimski et al., 2002; Chen et al., 2005). The two positive excursions in the late Frasnian were usually assumed as a result of enhanced organic carbon burial fraction (Joachimski and Buggisch, 1993; Joachimski et al., 2002; Chen et al., 2005). The enhanced burial of organic carbon likely resulted in a large and abrupt drop in atmospheric pCO_2 and thus may have contributed to climate cooling (Joachimski and Buggisch, 2002). This is supported by the observations that the positive shift in $\delta^{13}C_{carb}$ coincides with but predates the positive excursion of $\delta^{18}O_{PO_4}$ during the deposition of the UKH in the Yangdi (Fig. 2) and German sections (Joachimski and Buggisch, 2002).

The significant cooling may have initiated a short-term continental glaciation (Streel et al., 2000) and a major eustatic sea-level fall (Johnson et al., 1985). The eustatic sea-level fall would have caused exposure of carbonate platforms, accelerating coastal erosion and karstification (Chen and Tucker, 2004) and thus led to an increased riverine flux, which is supported by the elevated $^{87}Sr/^{86}Sr$ ratios measured on carbonates in the upper part of the UKH (Chen et al., 2005). Furthermore, global climate cooling would have increased equator-to-pole temperature gradient, favoring intensified oceanic circulation and upwelling (Song et al., 2017). Both mechanisms could lead to an increased nutrient delivery to shallow water environments in upwelling areas. Additionally, an elevated delivery of riverine nutrients flux to the oceans might have been favored by rapid colonization of continental areas by vascular land plants (Algeo and Scheckler, 1998). The nutrient pulse could have facilitated marine phytoplankton blooming (Gong et al., 2002) and resulted in an increased primary productivity, which is a potential cause for the positive excursion in $\delta^{13}C_{carb}$ in the UKH to have persisted during the Lower to Middle *Pa. triangularis* Zone (Joachimski et al., 2002; this study).

The coupling of $\delta^{13}C_{carb}$ and $\delta^{18}O_{PO_4}$ in the UKH at the Yangdi section is thus interpreted as a cause–effect link between the carbon cycling and climate change. However, this link cannot explain the positive shift in $\delta^{18}O_{PO_4}$ coinciding with an ongoing decrease in $\delta^{13}C_{carb}$ during the Upper *Pa. rhenana* Zone. The positive shift in $\delta^{18}O_{PO_4}$ in the Upper *Pa. rhenana* Zone at a position that correlated with the LKH is assumed as a global signal. The $\delta^{13}C_{carb}$ in the LKH generally displays a positive excursion (Joachimski and Buggisch, 1993; Joachimski et al., 2002), which was assumed as a global signal of variation in $\delta^{13}C_{DIC}$ (Joachimski et al., 2002). However, due to different local conditions, the positive excursion in $\delta^{13}C_{carb}$ associated with the LKH is vague in some areas, e.g., Casey Fall's section (Australia) (Joachimski et al., 2002) and Fuhe section (South China) (Chen et al., 2005). The decreasing trend in carbon isotope values in the Upper *Pa. rhenana* Zone at the Yangdi section was explained as a result of reduced organic carbon burial, which probably reflects local carbon cycling. As a result, the $\delta^{13}C_{carb}$ varied in a negative relationship with $\delta^{18}O_{PO_4}$ during the Upper *Pa. rhenana* Zone might reflect a local signal.

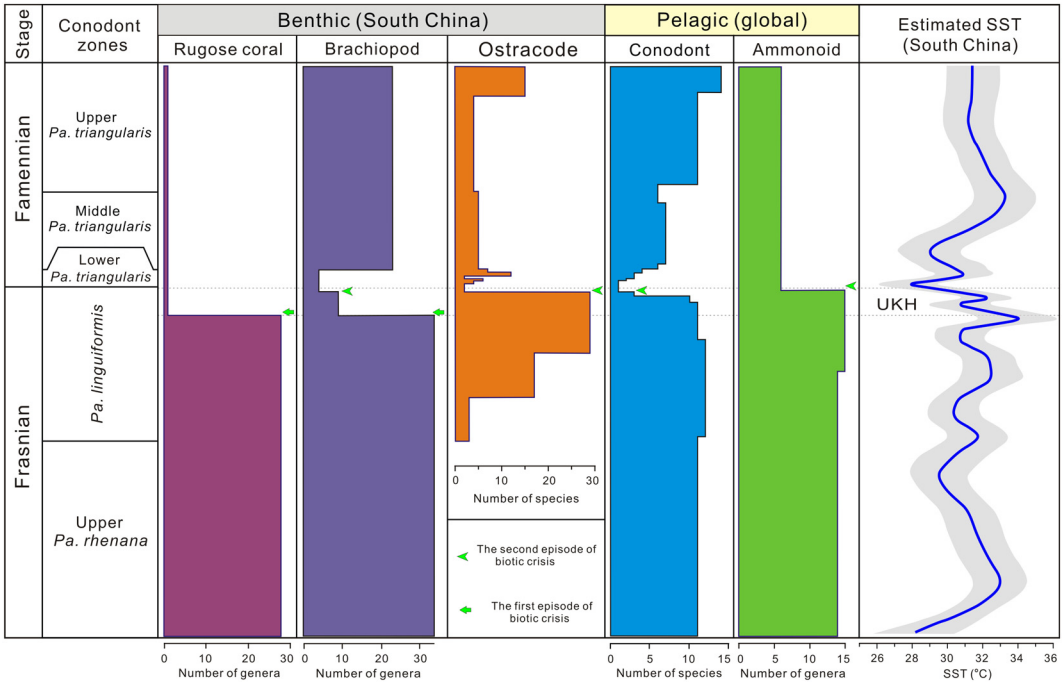

Fig. 7. Comparison of variations in diversity of major marine taxa, and sea surface water temperature (SST) based on $\delta^{18}O_{PO_4}$ records of conodonts across the Frasnian–Famennian boundary. Conodont data are from Huang and Gong (2016); ammonoid data are from Becker and House (1994); data of benthic faunas are from Ma et al. (2016); *Pa.—Palmatolepis*.

5.5. Relationship between climate changes and biotic crisis

It has been shown that the F–F biotic crisis not only severely affected the marine ecosystems but also decimated the terrestrial ecosystems to some degree (McGhee, 1996). In the marine realm, the ecological selectivity of the F–F biotic crisis seems to indicate that faunas adapted to warm temperatures suffered high losses, whereas faunas tolerating cooler water temperatures were less affected and were migrating into warm- or shallow-water environments (McGhee, 1996; Ma et al., 2016). For example, warm-adapted benthic ostracods were severely affected, while deep water solitary rugose corals and sponges seem to have been less affected (Ma et al., 2016). More than 90% of all brachiopod families from the low-latitude, tropical regions vanished, whereas brachiopods from the cooler water regions of Gondwana only suffered a loss of 27% (McGhee, 1996). Following the F–F biotic crisis, faunas (e.g. foraminifers) that were previously thriving in high-latitude areas were confined to low-latitude regions in the early Famennian, while the surviving low-latitude faunal groups experienced a substantial contraction in their latitudinal distribution (Kalvoda, 1990).

Most studies have revealed that the F–F (Kellwasser) biotic crisis was composed of a series of extinction pulses in conjunction with the deposition of the LKH and UKH (Schindler, 1993; McGhee, 1996; Huang and Gong, 2016; Ma et al., 2016), i.e., Lower and Upper Kellwasser Crisis. Quantitative fossil records constrained by conodont biostratigraphy reveal that two steps of the Upper Kellwasser Crisis are registered at the base and near the top of the UKH, respectively (Fig. 7). In contrast to the globally synchronous Upper Kellwasser Crisis, an exact timing of the Lower Kellwasser Crisis is still ambiguous in most areas. The metazoan reefs losses were not synchronous world-wide, but show a progressive stepwise decline within or below the Upper *Pa. rhenana* Zone (Copper, 2002). In South China, the sharp decline in coral-stromatoporoid reefs occurred in the Upper *Pa. rhenana* Zone (Ma et al., 2016), and thus it can be correlated with the climatic cooling during the deposition of the LKH.

Although it is generally accepted that the F–F biotic crisis was caused by Earth-bound mechanisms (e.g. oceanic anoxia, oceanic eutrophication, sea-level change, and hydrothermal activity; e.g. Johnson et al., 1985; Joachimski and Buggisch, 1993; Gong et al., 2002; Chen et al., 2005), these mechanisms cannot well explain the ecological selectivity of the F–F biotic crisis. For example, most mechanisms including oceanic anoxia (Joachimski and Buggisch, 1993), oceanic eutrophication (Gong et al., 2002), and sea-level changes (Johnson et al., 1985) cannot explain an impact on the terrestrial ecosystem. Furthermore, oceanic anoxia during the deposition of Kellwasser horizons has been confirmed as a regional phenomenon (Song et al., 2017). Additionally, the evidence for the hydrothermal activity during the F–F transition is too vague (e.g. Chen et al., 2005) to be responsible for the biocrisis. In contrast, the coincidence of the Kellwasser Crisis with global cooling suggests that climatic cooling played a major role in biodiversity reduction.

Global climate change may result in the geographical distribution of organisms, phenotypic changes, and evolutionary adaptation (Bijma et al., 2013; Hoffmann and Sgrò, 2011). If a population or species is unable to migrate or adapt fast enough to keep up with the rapid climate change, they will suffer a risk of lower speciation rates (Bijma et al., 2013; Hoffmann and Sgrò, 2011). The specialization of animals to a certain temperature range traditionally results from trade-offs in structural properties of enzymes or membranes and associated functional adjustments to temperature changes (Bijma et al., 2013). In case of climate cooling, warm-adapted animals are prone to a decrement in aerobic performance due to the limited functional capacity of oxygen supply systems to match oxygen demand (Bijma et al., 2013). From the viewpoint of genes, tropical climate specialists lack genetic variance for cold resistance presumably because the required alleles have been lost through DNA decay or pleiotropic selection (Hoffmann and Sgrò, 2011), which could reflect a low evolutionary potential. As a result, most low-latitude populations would have encountered survival pressure due to physiological limits and latitudinal compression of biogeographic ranges during the F–F climate cooling

(McGhee, 1996), whereas high-latitude or deep-water faunas could have survived climate cooling through migrating into low-latitude or shallow-water regions.

As indicated in the Late Ordovician, short-lived (~2 Myr) cooling by 5 °C may have caused mass extinction (Finnegan et al., 2011). The short-term (~0.2 Myr) 6 °C cooling during the deposition of the UKH suggests an even faster rate of climate change and might be more threatening to the survival of stenothermal species through reducing speciation rates. A lower speciation rate during the F–F transition has been confirmed by analyses of biogeographic and phylogenetic patterns of shallow water species (Stigall, 2012). Climate cooling during the latest Frasnian might have caused the taxonomic diversity decline in miospores (Streel et al., 2000). In contrast to the relatively fast climate cooling during the deposition of the UKH, the relatively slow cooling (~0.7 Myr) of ~3 °C during the deposition of the LKH probably did not result in a major decline in biodiversity except metazoan reefs. The Frasnian reef-dwelling faunas were assumed to be warm-adapted stenotherms (Copper, 2002) that were sensitive to climatic cooling. The timing and amplitude of the climatic cooling during the deposition of the LKH seems variable in different areas, which could explain why the decline in metazoan reefs was asynchronous.

6. Conclusions

The conodont apatite oxygen isotope record from the Yangdi section was used to reconstruct a detailed palaeotemperature history for South China as well as to reconstruct ecology of conodont taxa during the F–F transition. The high-resolution $\delta^{18}O_{PO_4}$ record based on mono-generic conodont samples exhibits a comparable long-term trend in comparison to published results from the western Palaeotethys, suggesting that these records document global temperature changes.

The identifiable differences in $\delta^{18}O_{PO_4}$ values between different conodont taxa indicate that *Palmatolepis* was likely to thrive in the uppermost part of water column, whereas *Polygnathus* and *Icriodus* may have lived at variable water-depths. The $\delta^{18}O_{PO_4}$ records measured on mono-generic samples suggested that the palaeoecological evidence of conodonts cannot be used to infer palaeoenvironments immediately after the mass extinction. Two cooling pulses are indicated by the increase in $\delta^{18}O_{PO_4}$ at the Lower (~0.7‰) and Upper Kellwasser horizons (~1.4‰), respectively, which is manifested as a global signal during the F–F transition. The concomitant changes in $\delta^{13}C_{carb}$ and $\delta^{18}O_{PO_4}$ in the Upper Kellwasser horizon suggested that climate change was controlled by the global carbon cycle (Joachimski and Buggisch, 2002). The temporal relationship between climate change and biodiversity decline suggests that the Kellwasser biotic crisis can be attributed to the effects of climate cooling.

Acknowledgements

We are grateful to Daniele Lutz for analyzing the oxygen isotope composition of conodont apatite. Haijun Song and two anonymous reviewers are thanked for their constructive comments. This work was financially supported by the National Natural Science Foundation of China (41290260, 41602027, 41472001), the 111 project (B08030), and National Science and Technology Major Projects (2016ZX05004002-001).

Appendix A. Supplementary material

Supplementary material related to this article can be found online at https://doi.org/10.1016/j.epsl.2018.05.016.

References

Algeo, T.J., Scheckler, S.E., 1998. Terrestrial-marine teleconnections in the Devonian: links between the evolution of land plants, weathering processes, and marine anoxic events. Philos. Trans. R. Soc. Lond. B, Biol. Sci. 353, 113–130.

Balter, V., Renaud, S., Girard, C., Joachimski, M.M., 2008. Record of climate-driven morphological changes in 376 Ma Devonian fossils. Geology 36, 907–910.

Becker, R.T., House, M.R., 1994. Kellwasser events and goniatite successions in the Devonian of the Montagne Noire with comments on possible causations. Cour. Forsch.inst. Senckenb. 169, 112–114.

Belka, Z., Wendt, J., 1992. Conodont biofacies patterns in the Kellwasser facies (Upper Frasnian/Lower Famennian) of the eastern Anti-Atlas, Morocco. Palaeogeogr. Palaeoclimatol. Palaeoecol. 91, 143–173.

Bijma, J., Pörtner, H.O., Yesson, C., Rogers, A.D., 2013. Climate change and the oceans—what does the future hold? Mar. Pollut. Bull. 74, 495–505.

Boucot, A.J., Scotese, C.R., Chen, X., Morley, R.J., 2013. Phanerozoic Paleoclimate: An Atlas of Lithologic Indicators of Climate. Society for Sedimentary Geology, Tulsa. 478 pp.

Buggisch, W., Joachimski, M.M., Sevastopulo, G., Morrow, J.R., 2008. Mississippian $\delta^{13}C_{carb}$ and conodont apatite $\delta^{18}O$ records—their relation to the Late Palaeozoic Glaciation. Palaeogeogr. Palaeoclimatol. Palaeoecol. 268, 273–292.

Chen, D.Z., Qing, H.R., Li, R.W., 2005. The Late Devonian Frasnian–Famennian (F/F) biotic crisis: insights from $\delta^{13}C_{carb}$, $\delta^{13}C_{org}$ and $^{87}Sr/^{86}Sr$ isotopic systematics. Earth Planet. Sci. Lett. 235, 151–166.

Chen, D.Z., Tucker, M.E., 2004. Palaeokarst and its implication for the extinction event at the Frasnian–Famennian boundary (Guilin, South China). Mem. Geol. Soc. Lond. 161, 895–898.

Copper, P., 2002. Reef development at the Frasnian/Famennian mass extinction boundary. Palaeogeogr. Palaeoclimatol. Palaeoecol. 181, 27–65.

Donoghue, P.C.J., Forey, P.L., Aldridge, R.J., 2000. Conodont affinity and chordate phylogeny. Biol. Rev. Camb. Philos. Soc. 75, 191–251.

Finnegan, S., Bergmann, K., Eiler, J.M., Jones, D.S., 2011. The magnitude and duration of Late Ordovician–Early Silurian glaciation. Science 331, 903–906.

Gong, Y.M., Li, B.H., Si, Y.L., Wu, Y., 2002. Late Devonian red tide and mass extinction. Chin. Sci. Bull. 47, 1138–1144.

Gong, Y.M., Li, B.H., Wang, C.Y., Wu, Y., 2001. Orbital cyclostratigraphy of the Devonian Frasnian–Famennian transition in South China. Palaeogeogr. Palaeoclimatol. Palaeoecol. 168, 237–248.

Henkes, G.A., Passey, B.H., Grossman, E.L., Shenton, B.J., Yancey, T.E., Pérez-Huerta, A., 2018. Temperature evolution and the oxygen isotope composition of Phanerozoic oceans from carbonate clumped isotope thermometry. Earth Planet. Sci. Lett. 490, 40–50.

Hoffmann, A.A., Sgrò, C.M., 2011. Climate change and evolutionary adaptation. Nature 470, 479–485.

Houedec, S.L., Girard, C., Balter, V., 2013. Conodont Sr/Ca and $\delta^{18}O$ record seawater changes at the Frasnian–Famennian boundary. Palaeogeogr. Palaeoclimatol. Palaeoecol. 376, 114–121.

Huang, C., Gong, Y.M., 2016. Timing and patterns of the Frasnian–Famennian event: evidences from high-resolution conodont biostratigraphy and event stratigraphy at the Yangdi section, Guangxi, South China. Palaeogeogr. Palaeoclimatol. Palaeoecol. 448, 317–338.

Ihaka, R., Gentleman, R., 1996. A language for data analysis and graphics. J. Comput. Graph. Stat. 5, 299–314.

Jaffrés, J.B.D., Shields, G.A., Wallmann, K., 2007. The oxygen isotope evolution of seawater: a critical review of a long-standing controversy and an improved geological water cycle model for the past 3.4 billion years. Earth-Sci. Rev. 83, 83–122.

Joachimski, M.M., Breisig, S., Buggisch, W., Talent, J.A., 2009. Devonian climate and reef evolution: insights from oxygen isotopes in apatite. Earth Planet. Sci. Lett. 284, 599–609.

Joachimski, M.M., Buggisch, W., 1993. Anoxic events in the Late Frasnian—causes of the Frasnian–Famennian faunal crisis? Geology 21, 675–678.

Joachimski, M.M., Buggisch, W., 2002. Conodont apatite $\delta^{18}O$ signatures indicate climatic cooling as a trigger of the Late Devonian mass extinction. Geology 30, 711–714.

Joachimski, M.M., Pancost, R.D., Freeman, K.H., Ostertag-Henning, C., Buggisch, W., 2002. Carbon isotope geochemistry of the Frasnian–Famennian transition. Palaeogeogr. Palaeoclimatol. Palaeoecol. 181, 91–109.

Johnson, J.G., Klapper, G., Sandberg, C.A., 1985. Devonian eustatic fluctuations in Euramerica. Geol. Soc. Am. Bull. 96, 567–587.

Kalvoda, J., 1990. Late Devonian–Early Carboniferous paleobiogeography of benthic foraminifera and climatic oscillations. In: Kauffman, E.G., Walliser, O.H. (Eds.), Extinction Events in Earth History. Springer, Berlin, Heidelberg, pp. 183–187.

Kolodny, Y., Luz, B., Navon, O., 1983. Oxygen isotope variations in phosphate of biogenic apatites, I. Fish bone apatite—rechecking the rules of the game. Earth Planet. Sci. Lett. 64, 398–404.

Lécuyer, C., Allemand, P., 1999. Modelling of the oxygen isotope evolution of seawater: implications for the climate interpretation of the $\delta^{18}O$ of marine sediments. Geochim. Cosmochim. Acta 63, 351–361.

Lécuyer, C., Amiot, R., Touzeau, A., Trotter, J., 2013. Calibration of the phosphate $\delta^{18}O$ thermometer with carbonate–water oxygen isotope fractionation equations. Chem. Geol. 347, 217–226.

Lécuyer, C., Grandjean, P., O'Neil, J.R., Cappetta, H., Martineau, F., 1993. Thermal excursions in the ocean at the Cretaceous–Tertiary boundary (northern Morocco): $\delta^{18}O$ record of phosphatic fish debris. Palaeogeogr. Palaeoclimatol. Palaeoecol. 105, 235–243.

Loader, C.R., 1999. Local Regression and Likelihood. Springer, Berlin. 290 pp.

Ma, X.P., Gong, Y.M., Chen, D.Z., Racki, G., Chen, X.Q., Liao, W.H., 2016. The Late Devonian Frasnian–Famennian event in South China—patterns and causes of extinctions, sea level changes, and isotope variations. Palaeogeogr. Palaeoclimatol. Palaeoecol. 448, 224–244.

McGhee, G.R., 1996. The Late Devonian Mass Extinction. Columbia University Press, New York. 303 pp.

Muehlenbachs, K., 1998. The oxygen isotopic composition of the oceans, sediments and the seafloor. Chem. Geol. 145, 263–273.

Nöth, S., 1998. Conodont color (CAI) versus microcrystalline and textural changes in Upper Triassic conodonts from Northwest Germany. Facies 38, 165–173.

Paul, D., Skrzypek, G., Fórizs, I., 2007. Normalization of measured stable isotopic compositions to isotope reference scales—a review. Rapid Commun. Mass Spectrom. 21, 3006–3014.

Pucéat, E., Joachimski, M.M., Bouilloux, A., Monna, F., Bonin, A., Motreuil, S., Morinière, P., Hénard, S., Mourin, J., Dera, G., Quesne, D., 2010. Revised phosphate–water fractionation equation reassessing paleotemperatures derived from biogenic apatite. Earth Planet. Sci. Lett. 298, 135–142.

Pucéat, E., Reynard, B., Lécuyer, C., 2004. Can crystallinity be used to determine the degree of chemical alteration of biogenic apatites? Chem. Geol. 205, 83–97.

Rejebian, V.A., Harris, A.G., Huebner, J.S., 1987. Conodont colour and textural alteration: an index to regional metamorphism, contact metamorphism and hydrothermal alteration. Geol. Soc. Am. Bull. 99, 471–497.

Retallack, G.J., Hunt, R.R., White, T.S., 2009. Late Devonian tetrapod habitats indicated by palaeosols in Pennsylvania. Mem. Geol. Soc. Lond. 166, 1143–1156.

Sandberg, C.A., Morrow, J.R., Ziegler, W., 2002. Late Devonian sea-level changes, catastrophic events, and mass extinctions. Spec. Pap., Geol. Soc. Am. 356, 473–487.

Sandberg, C.A., Ziegler, W., Dreesen, R., Butler, J.L., 1989. Late Frasnian mass extinction: conodont event stratigraphy, global changes, and possible causes. Cour. Forsch.inst. Senckenb. 102, 263–307.

Savin, S., 1977. The history of the Earth's surface temperature during the past 100 million years. Annu. Rev. Earth Planet. Sci. 5, 319–355.

Schindler, E., 1993. Event-stratigraphic markers within the Kellwasser crisis near the Frasnian/Famennian boundary (upper Devonian) in Germany. Palaeogeogr. Palaeoclimatol. Palaeoecol. 104, 115–125.

Schrag, D.P., Hampt, G., Murray, D.W., 1996. Pore fluid constraints on the temperature and oxygen isotopic composition of the glacial ocean. Science 272, 1930–1932.

Shemesh, A., 1990. Crystallinity and diagenesis of sedimentary apatites. Geochim. Cosmochim. Acta 54, 2433–2438.

Song, H.Y., Song, H.J., Algeo, T.J., Tong, J., Romaniello, S.J., Zhu, Y., Chu, D., Gong, Y., Anbar, A.D., 2017. Uranium and carbon isotopes document global-ocean redox-productivity relationships linked to cooling during the Frasnian–Famennian mass extinction. Geology 45, 887–890.

Stigall, A.L., 2012. Speciation collapse and invasive species dynamics during the Late Devonian "mass extinction". GSA Today 22, 4–9.

Streel, M., Caputo, M.V., Loboziak, S., Melo, J.H.G., 2000. Late Frasnian–Famennian climates based on palynomorph analyses and the question of the Late Devonian glaciations. Earth-Sci. Rev. 52, 121–173.

Thomas, D.B., Fordyce, R.E., Frew, R.D., Gordon, K.C., 2007. A rapid, non-destructive method of detecting diagenetic alteration in fossil bone using Raman spectroscopy. J. Raman Spectrosc. 38, 1533–1664.

Trotter, J.A., Gerald, J.D.F., Kokkonen, H., Barnes, C.R., 2007. New insights into the ultrastructure, permeability, and integrity of conodont apatite determined by transmission electron microscopy. Lethaia 40, 97–110.

Trotter, J.A., Williams, I.S., Nicora, A., Mazza, M., Rigo, M., 2015. Long-term cycles of Triassic climate change: a new $\delta^{18}O$ record from conodont apatite. Earth Planet. Sci. Lett. 415, 165–174.

Van Geldern, R., Joachimski, M.M., Day, J., Jansen, U., Alvarez, F., Yolkin, E.A., Ma, X.P., 2006. Carbon, oxygen and strontium isotope records of Devonian brachiopod shell calcite. Palaeogeogr. Palaeoclimatol. Palaeoecol. 240, 47–67.

Veizer, J., Prokoph, A., 2015. Temperatures and oxygen isotopic composition of Phanerozoic oceans. Earth-Sci. Rev. 146, 92–104.

Vennemann, T.W., Fricke, H.C., Blake, R.E., O'Neil, J.R., Colman, A., 2002. Oxygen isotope analysis of phosphates: a comparison of techniques for analysis of Ag_3PO_4. Chem. Geol. 185, 321–336.

Wenzel, B., Lécuyer, C., Joachimski, M.M., 2000. Comparing oxygen isotope records of Silurian calcite and phosphate—$\delta^{18}O$ compositions of brachiopods and conodonts. Geochim. Cosmochim. Acta 64, 1859–1872.

Xu, R., Gong, Y., Zeng, J., 2008. Coupling relationships between brachiopods and Girvanella during the Late Devonian F–F transition in Guilin, South China. Sci. China, Ser. D 51, 1581–1588.

Zazzo, A., Lécuyer, C., Mariotti, A., 2004. Experimentally-controlled carbon and oxygen isotope exchange between bioapatites and water under inorganic and microbially-mediated conditions. Geochim. Cosmochim. Acta 68, 1–12.